Indian Journal of Fibre & Textile Research
Vol. 43, September 2018, pp. 301-307

Evaluation of flexural modulus of carbon 3D orthogonal woven fabric using a trilinear model

Shohreh Minapoor, Saeed Ajeli[a] & Mohammad Sheikhzadeh

Department of Textile Engineering, Isfahan University of Technology, Isfahan, Iran

Received 12 November 2016; revised received and accepted 14 February 2017

Bending behaviour of 3D orthogonal carbon weave composite reinforcement has been investigated. The three-point bending test method has been employed and the load-deflection curves are examined. The influence of carbon fibre tow type, yarn insertion and tension of longitudinal yarns on fibre volume fraction and bending properties of non-crimp 3D orthogonal carbon weave is discussed. It is found that carbon fibre bending properties due to cross-section shape and geometry have a great impact on bending behavior of non-crimp 3D orthogonal carbon weave. Increasing the number of transversal yarns layers and tension of longitudinal yarns increases both fibre volume fraction and bending modulus of non-crimp 3D orthogonal carbon weave. From the bending properties calculated, the factors for improving fibre volume fraction and bending behavior of non-crimp 3D orthogonal carbon weaves are discussed.

Keywords: 3D Orthogonal weave, Carbon fibres, Flexural modulus, Non-crimp fabric, Three-point bending , Trilinear model, Woven fabric

1 Introduction

3D woven composite materials are increasingly main options for many types of structures, such as aircrafts, missiles, armor protection, etc. The fibre architecture of 3D orthogonal woven fabrics consists of in-plane layers of warp and weft yarns interlocked with z-binder yarns in the through-thickness direction. Researchers have shown that the z-binders improved the delamination resistance, impact damage resistance, fracture toughness and post-impact mechanical properties of the 3D orthogonal woven composites[1-3]. In a non-interlacing orthogonal fabric, all warps, wefts and fill-directional yarns remain practically straight in structure[4]. This feature distinguishes this kind of weave from conventional 2D woven fabrics which are crimped as all warp and weft yarns are interlaced. As significantly higher in-plane stiffness and strength can be achieved in a no-crimp fabric, non-crimp 3D orthogonal structure is obviously beneficial for composite reinforcement[5-7]. Mechanical behavior of a 3D reinforcement plays a key role in the definition of the fibre orientations, which influences the permeability of preform and finally defines the mechanical quality of a composite component. In spite of many attempts to study and model the mechanical behavior of composites reinforced with non-crimp 3D orthogonal fabrics[8-10], the mechanical properties of these reinforcements are not deeply known and investigated.

Recently, Mishra *et al.*[11] have focused on geometric and micromechanical modeling of non-crimp 3D orthogonal fabrics for composite applications and proposed meso-finite element model. Shi *et al.*[12] have presented an analytical model to compute the energy absorption of non-crimp 3D orthogonal fabric under ballistic penetration of a rigid projectile and stated the greater potential applications of this weave in ballistic protection. Also, the ballistic impact damages on 3D orthogonal woven fabric were investigated through experimental analysis and finite-element simulations by Jia *et al.*[13] Carvelli *et al.*[14] have experimentally investigated the deformability of a single-ply E-glass non-crimp 3D orthogonal woven reinforcement. They have focused on the understanding and measurement of the main deformation modes, in-plane biaxial tension and shear behavior, which are involved during draping of composite reinforcements.

The behavior of non-crimp 3D orthogonal woven reinforcement due to the specific geometry of Z-binding and extreme straightness of the stuffing warp and weft yarns is quite different from the tight

[a]Corresponding author.
E-mail: sajeli@cc.iut.ac.ir

heavily interlaced angle interlock weaves[14]. Detailed analysis of the mechanical behavior of this reinforcement indicates the fabric behavior and performance in composite manufacturing process and its technical applications. The aim of the current work is to study the bending behavior of a carbon non-crimp 3D orthogonal woven reinforcement experimentally. Non-crimp 3D orthogonal carbon samples with different weave parameters are subjected to a three-point bending test and bending properties are obtained. The influence of yarn and structure parameters on fibre volume fraction and bending behavior of non-crimp 3D orthogonal carbon fabric is also discussed.

2 Materials and Methods

2.1 Materials

Two carbon fibre tows types (Torayca, America Inc) were used for weaving the non-crimp 3D orthogonal weave samples produced on a self-designed loom based on uniaxial noobing process[4]. Tables 1 and 2 show the specifications of carbon fibre tows and the non-crimp 3D orthogonal samples respectively. The warp and weft insertion densities are varied in two levels (1 and 2 layers per centimeter). Also, the tension of longitudinal yarns is defined in two terms, namely no-stress state and pre-stress state. No-stress state means the longitudinal yarns (Z-yarns) set on the loom smoothly and without any stretching. In pre-stress state, 6K and 12K carbon tows are subjected to 120 and 200 N force respectively according to their force-elongation curves and then weaving process is done. Photographs of non-crimp 3D orthogonal carbon samples and the difference between two yarn types, and warp and weft yarns insertion densities are shown in Fig. 1.

2.2 Calculation of Preform Volume Fraction

The fraction of fibre reinforcement is very important in determining the overall mechanical properties of a composite. A higher fibre volume fraction (FVF) typically results in better mechanical properties of the composite[15]. To determine FVF of non-crimp 3D orthogonal carbon samples, two methods were used. In the first method, FVF was measured from volume and mass of samples using the following equation:

$$FVF = \frac{V_f}{V_t} \times 100 \quad \text{... (1)}$$

Table 1 — Properties of carbon fibres

Fibre	Number of filaments	Tensile modulus $\times 10^9$, N/m^2	Elongation %	Density g/cm^3	Yield g/1000m
T300	6000	124.9 (5)	1.6 (6)	1.7 (1)	400 (3)
T300	12000	126.0 (5)	2.0 (9)	1.7 (8)	800 (5)

Numbers in parentheses show coefficient of variation %.

Table 2 — Specifications of non-crimp 3D orthogonal carbon samples

Sample code[a]	Yarns	Number of filaments	Insertion density ends/ cm	Layers/ cm	Z-yarns tension[b]
6K1D	Warp/ Weft	6K	8	1	N
	Z-yarn	6K	16	8	N
6K2D	Warp/ Weft	6K	16	2	N
	Z-yarn	6K	16	8	N
6K1D/S	Warp/ Weft	6K	8	1	N
	Z-yarn	6K	16	8	S
6K2D/S	Warp/ Weft	6K	16	2	N
	Z-yarn	6K	16	8	S
12K1D	Warp/ Weft	12K	8	1	N
	Z-yarn	12K	16	8	N
12K2D	Warp/ Weft	12K	16	2	N
	Z-yarn	12K	16	8	N
12K1D/S	Warp/ Weft	12K	8	1	N
	Z-yarn	12K	16	8	S
12K2D/S	Warp/ Weft	12K	16	2	N
	Z-yarn	12K	16	8	S

[a]6K and 12K carbon fibre tow, 1D–1 layer/cm warp/weft insertion density, 2D–2 layers / cm warp/weft insertion density and S–pre-stress of longitudinal yarns.

[b]N– No-stress state and S–Pre-stress state.

where FVF, V_f and V_t represent the fibre volume fraction (%), volume of fibres (cm^3) and volume of sample (cm^3) respectively. The volume of fibres was calculated using the weight of samples and density of carbon tow. In the second method, fibre volume fraction was determined by calculating the weight of fibres in a 1×1×1 cm^3 volume unit. The weight of fibres in the volume unit or sample density was obtained using a number of clues, length and linear density of yarns. Then, fibre volume fraction was measured using the following equation:

$$\text{FVF} = \frac{\rho_t}{\rho} \times 100 \quad \text{…(2)}$$

where ρ_t and ρ represent a sample and carbon tow density (g/cm^3) respectively.

The terminal spines on the edges of non-crimp 3D orthogonal samples make the sample size and volume greater than the actual value. So, the width and thickness of sample were measured using digital images regardless terminal spines on the edges (Fig. 2). FVF was calculated in two states, namely by foreseeing terminal spines and without them

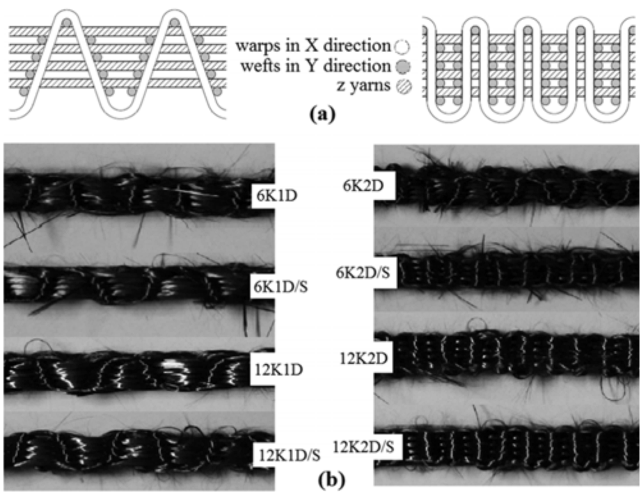

Fig. 1 — Non-crimp 3D orthogonal performs (a) chematic of warp and weft densities in weave's cross-section and (b) 6K and 12K samples with different layers per cm warp and weft densities

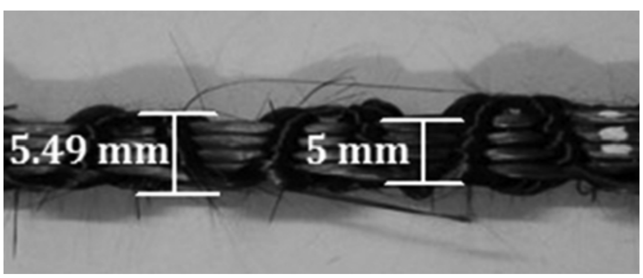

Fig. 2 — Measuring the width of a non-crimp 3D orthogonal preform using digital images regardless terminal spines on the edges

(called "total FVF" and "actual FVF" respectively). The result of FVF is given in Table 3.

2.3 Three-point Bending Test

As can be seen, non-crimp orthogonal samples are three dimensional and rigid. Measuring their bending properties with Shirley stiffness tester, like 2D fabric samples, is impossible[16]. So, for investigating bending properties of non-crimp 3D orthogonal samples, three-point bending test was used according to ASTM D790. The test was conducted on a Zwick universal testing machine (Type: 144660) and the support span-to-depth ratio was set 16:1. As shown in Fig. 3, the sample was positioned symmetrically on two supporting rollers with spacing of 80 mm, enabling an even amount of force to be applied to each sample. The pressing roller was located at the center of the top surface and is then lowered at a constant speed of 2 mm/min to deform the sample, causing it to bend until a 10 mm displacement achieved. This test was conducted three times for each sample and load–deflection plots were obtained for each test.

3 Results and Discussion

The bending results were plotted in terms of applied load versus center displacement of the sample under the crosshead of the tester machine. Figure 4 shows load-deflection curves of 12K2D/S samples.

According to ASTM D790, the bending stress, strain and modulus are calculated using the following equations:

$$S = \frac{3PL}{2bd^2} \quad \ldots(3)$$

$$r = \frac{6Dd}{L^2} \quad \ldots(4)$$

Table 3 — Characterization and bending results of specimens

Specimen code	Density g/cm^3	Actual FVF %	Total FVF %	FVF		Initial slope	Bending modulus MPa
				Z direction %	X,Y direction %		
6K1D-1	0.89 (3.9)	68.04 (0.4)	50.29 (4.2)	26.33 (4.2)	11.98 (7.9)	0.41 (5.7)	54.97 (6.7)
6K2D-1	1.01 (3.6)	71.22 (0.4)	56.20 (2.5)	22.31 (1.7)	16.95 (3.1)	1.33 (9.1)	130.29 (7.7)
6K1D/S-1	0.94 (4.8)	70.67 (0.3)	52.80 (4.9)	27.27 (1.8)	12.77 (8.3)	0.89 (9.0)	128.11 (6.7)
6K2D/S-1	1.00 (0.6)	73.92 (0.5)	56.37 (0.8)	23.01 (1.7)	16.67 (0.9)	1.68 (8.4)	171.25 (4.0)
12K1D-1	1.08 (6.7)	86.20 (0.3)	61.74 (6.6)	21.47 (3.6)	20.14 (8.3)	0.41 (5.1)	35.34 (4.4)
12K2D-1	1.12 (1.8)	90.95 (0.3)	64.23 (1.5)	16.27 (0.2)	23.98 (2.0)	1.15 (5.6)	57.45 (6.5)
12K1D/S-1	1.09 (5.6)	88.91 (0.3)	62.49 (5.5)	21.81 (0.9)	20.34 (8.5)	0.59 (12.6)	52.26 (10.9)
12K2D/S-1	1.13(2.7)	93.73 (0.4)	64.65 (2.4)	16.50 (1.3)	24.08 (3.1)	1.43 (4.6)	72.94 (7.2)

Numbers in parentheses show coefficient of variation, %.

$$E_B = \frac{L^3 m}{4bd^3} \qquad \ldots(5)$$

where S is the stress in the outer fibres at Midspan (MPa); P, the load at a given point on the load-deflection curve (N); L, the support span (mm); d, the depth of the specimen (mm); b, the width of the specimen (mm); r, the maximum strain in the outer fibres (mm/mm); D, the maximum deflection of the center of the beam (mm); E_B, the modulus of elasticity in bending (MPa); m, the slope of the tangent to the initial straight-line portion of the load-deflection curve (N/mm).

As can be seen in Fig. 4, the initial straight-line portion of the load-deflection curve of non-crimp 3D orthogonal carbon sample is not clear such as load-deflection curves of metals and composites. Previous studies on investigating three-point bending of materials, such as plastics, composites, metals, ceramics and wood, show a clear straight-line portion of the load-deflection curve[17-20]. In such cases, it is easy to obtain the slope for calculating the modulus of elasticity in bending by fitting a proper line. However, it was difficult to distinguish the initial straight-line portion of the load-deflection curve of non-crimp 3D orthogonal carbon samples due to their forms and analysis of such curves haven't been done yet. So, in this work an attempt has been made by a trilinear model to determine the initial straight-line portion of curve and fit an appropriate straight-line.

3.1 Trilinear Model for Calculating Modulus

For ductile materials such as many aluminum alloys, copper, etc., the stress-strain diagram may be nonlinear from initial loading until final failure, as shown in Fig. 5. However, for small stresses and strains, a portion may be well approximated by a straight line and an approximate proportional limit

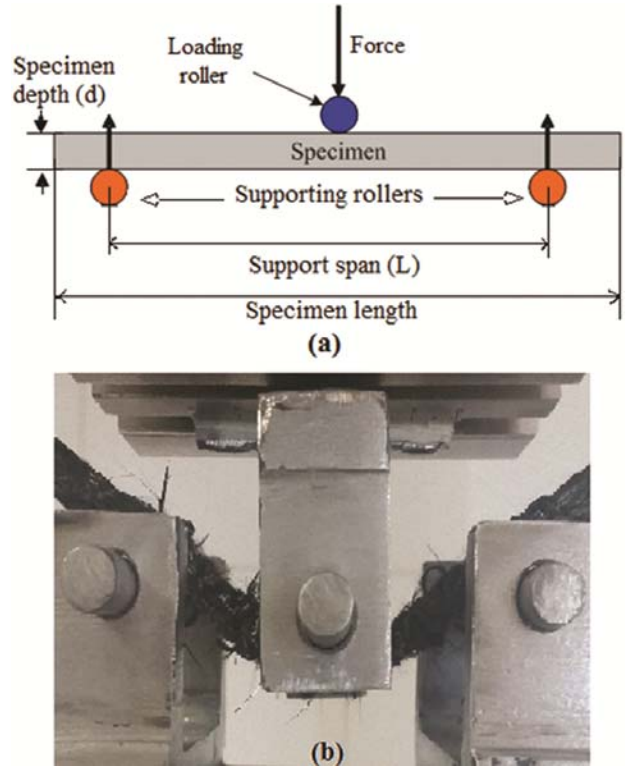

Fig. 3 — Three-point bending test (a) load configuration and (b) a non-crimp 3D orthogonal carbon specimen subjected to bending test

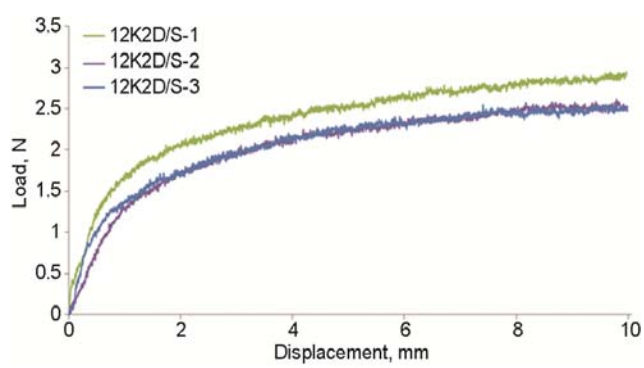

Fig. 4 — Load-deflection curves of 12K2D/S samples

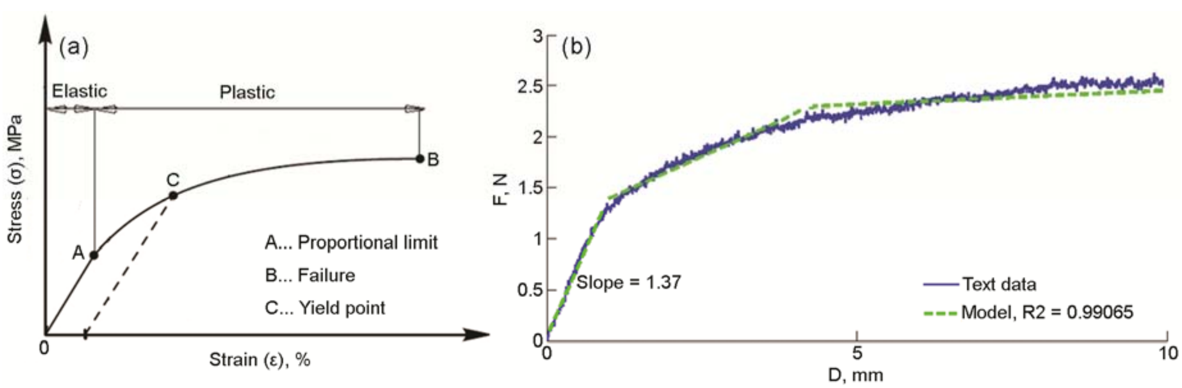

Fig. 5 — (a) Stress-strain diagram for ductile materials[21] and (b) Load-deflection curve of 12K2D/S-2 modeled with trilinear mode

(point A) can be determined. For many metals and other materials, if the stress exceeds the proportional limit a residual or permanent deformation may remain when the specimen is unloaded and the material is said to have “yielded” (point C). Above the yield stress, the material behaves plastically. At the lowest level of strain (from A to C) the material becomes stronger as the applied stress must increase in order to keep the material deforming. At high levels of strain (from C to B) the material flows under a constant stress[21].

According to the description given, triple points A, B and C are used for separating three regions of the load-deflection curve of non-crimp 3D orthogonal carbon sample in a trilinear model. A MATLAB code has been developed for fitting the best lines in these three areas. So, by detecting the best lines with the most correlation coefficients (R^2), the triple points are designated. Figure 5 shows the load-deflection curve of 12K2D/S-2 with trilinear model fitting on it. Using this model, the best initial straight-line portion of curve is determined and the slope of linear fitted line is extracted to calculate modulus of elasticity in bending. It should be noted that stress strain curves [conversion loud-deflection to stress-strain using Eqs (3) and (4)] can be modeled in this method. In this case, the slope of the initial straight-line fitted on the curve is the modulus of elasticity in bending.

Table 4 — Duncan analysis for comparison means of total FVF

Sample code	N	Subset for alpha = 0.05		
		1	2	3
6K1D	3	50.2864		
6K2D	3	52.8018	52.8018	
6K1D/S	3		56.1981	
6K2D/S	3		56.3646	
12K1D	3			61.7423
12K2D	3			62.4873
12K1D/S	3			64.2291
12K2D/S	3			64.6507
Sig.		0.214	0.101	0.187

3.2 Experimental and Statistical Analysis

Table 3 presents the measured characterization of specimens and bending results. In the first step, ANOVA analysis is carried out at 95% significance level to investigate the statistical effect of different parameters on FVF and modulus of elasticity in bending as response parameters. Obtained results show that all three parameters namely carbon fibre tow type, warp and weft insertion densities and longitudinal yarns tension (Z-yarns) have a significant effect on FVF and modulus of elasticity in bending.

Then, in discussing critical difference values for particular comparisons of means, Duncan analysis is carried out at 95% significance level. Tables 4-6 show the Duncan analysis for comparison means of total FVF, actual FVF and bending modulus of samples respectively. For more accurate analysis of the results, the effect of different parameters on FVF and modulus of elasticity in bending is separately investigated.

3.3 Effect of Weave Parameters on FVF

According to Table 4, there is a significant difference between total FVF of 3D samples woven with 6K and 12K carbon fibre tows. Clearly, the number of monofilaments increase leads to FVF increase. It can be seen that the effect of warp and weft insertion densities and longitudinal yarns tension (Z-yarns) only is significant in samples woven with 6K carbon fibre. Doubling the number of monofilaments in 12K carbon fibre tow will decrease the roll of warp and weft insertion densities and

Table 5 — Duncan analysis for comparison means of actual FVF

Sample code	N	Subset for alpha = 0.05							
		1	2	3	4	5	6	7	8
6K1D	3	68.0389							
6K1D/S	3		70.6740						
6K2D	3			71.2246					
6K2D/S	3				73.9178				
12K1D	3					86.2051			
12K1D/S	3						88.9124		
12K2D	3							90.9494	
12K2D/S	3								93.7332
Sig.		1.000	1.000	1.000	1.000	1.000	1.000	1.000	1.000

longitudinal yarns tension (Z-yarns) in FVF increasing. In both 6K and 12K carbon fibres, the more longitudinal yarns tension before weaving leads to FVF increment. It can be explained that the increase in longitudinal yarns tension causes setting the yarns more regularly and so decreasing the volume of sample. According to Table 5, there is a significant difference among the actual FVF of 3D samples woven with all variable parameters.

3.4 Effect of Weave Parameters on E_B

As is clear in Table 3, the orthogonal 3D samples woven with 6K carbon fibre have more bending rigidity. It is expected that the bending modulus of non-crimp 3D orthogonal sample increases by adding the number of carbon monofilaments and FVF of 3D samples, but the results show otherwise. So, the roll of yarn type is proposed regarding its shape and geometry. This parameter has a direct effect on behavior of yarn in bending because of great influence on moment of inertia. The results of Shirley bending tester show that 6K carbon fibre tow, used in this work, has a bending length equal to double of its value for a 12K carbon fibre tow. Table 6 shows that variety in type of carbon fibre tows has a great effect on bending modulus of non-crimp 3D orthogonal carbon weave. There is no significant difference among E_B of 6K1D, 12K2D and 12K1D/S, even by increasing warp and weft insertion densities and longitudinal yarns tension. It can be concluded that increasing the number of monofilaments in carbon tow without considering the cross-section shape of yarns, certainly will not increase the bending modulus of non-crimp 3D orthogonal carbon weave. According to Table 6, there is a significant difference among E_B in all 3D samples except 12K1D/S, 6K1D, 12K2D as well as 6K2D and 6K1D/S. No significant difference between 6K2D & 6K1D/S and between 12K2D &

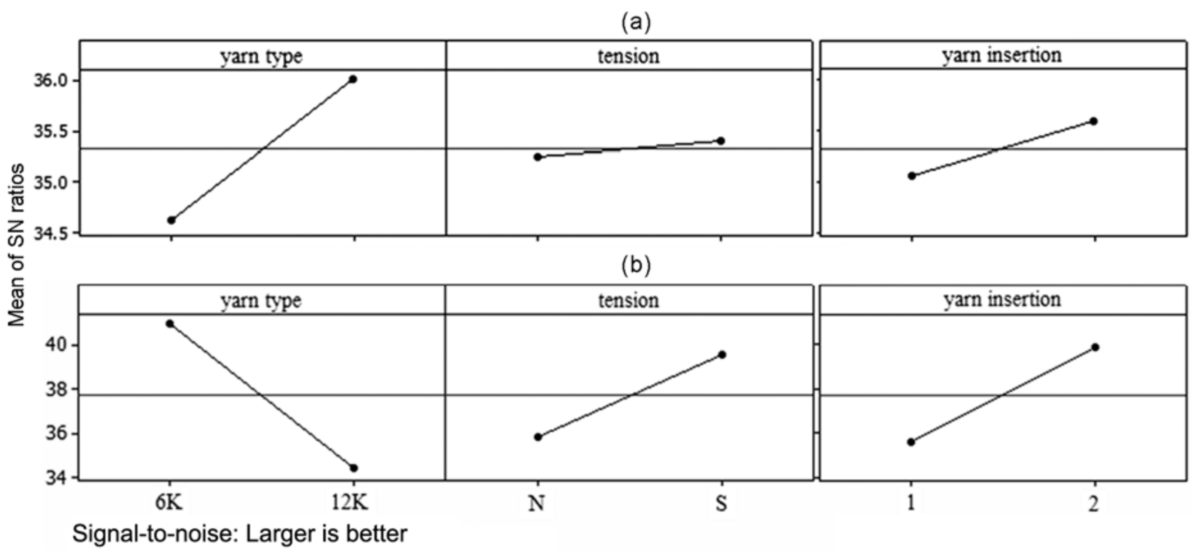

Fig. 6 — Main effects plots for SN ratios (a) FVF and (b) bending modulus

Table 6 — Duncan analysis for comparison means of bending modulus

Sample code	N	Subset for alpha = 0.05				
		1	2	3	4	5
12K1D	3	35.3445				
12K1D/S	3		52.2557			
6K1D	3		54.9676			
12K2D	3		57.4508			
12K2D/S	3			72.9408		
6K1D/S	3				128.1061	
6K2D	3				130.2923	
6K2D/S	3					171.2492
Sig.		1.000	0.349	1.000	0.674	1.000

12K1D/S indicates the marvelous equal effect of warp and weft insertion densities and longitudinal yarns tension on E_B.

3.5 Optimization Product Parameters for Better Bending Modulus

According to Taguchi's method, a larger-the-better analysis has been selected, i.e. the larger the FVF, the better is the bending modulus. The SN ratio (signal to nose ratio) analysis was adopted to identify the strongest effects and to determine the best factor levels for producing non-crimp 3D orthogonal carbon weave that have considerably more FVF and bending modulus. Furthermore, the optimum weave parameters to achieve the most FVF and modulus of elasticity in bending were determined. The results are similar for both feature FVF and E_B. Type of carbon fibre tow has the largest effect on the FVF and bending modulus of non-crimp 3D orthogonal carbon weave; warp and weft insertion density is next and followed by longitudinal yarns tension. The optimum conditions are summarized in Fig. 6. Use of 12K carbon fibre tow in producing non-crimp 3D orthogonal weaves yields more FVF. Weaving non-crimp 3D orthogonal samples with 6K carbon fibre tow, used in this work, results in higher weave's bending rigidity regarding sizing type and so higher bending length.

4 Conclusion

This study investigated the bending behaviour of 3D orthogonal carbon weave composite reinforcement. The results show that increase in the weft and warp yarn insertion density and longitudinal yarns tension leads to increase in fibre volume fraction and bending modulus of non-crimp 3D orthogonal carbon weave. While, adding the number of monofilaments of carbon tow does not increase the bending modulus presently. The bending rigidity of non-crimp 3D orthogonal carbon weave strongly depends on the cross-section shape and geometry of carbon tow and therefore yarn bending rigidity. According to Taguchi's method, the type of carbon fibre tow has the largest effect on the fibre volume fraction and bending modulus of non-crimp 3D orthogonal carbon weave; warp and weft insertion density is next which is followed by longitudinal yarns tension.

References

1 Mouritz A P, Bannisterb M K, Falzonb P J & Leongb K H, *Composites: Part A*, 30(1999) 1445.

2 Bilisik K, *Fibres Text East Eur*, 17(2009) 63.

3 Singletary J & Bogdanovich A, *J Ind Text*, 29(2000) 287.

4 Behera B K & Mishra R, *Indian J Fibre Text Res*, 33(2008) 274.

5 Unal P G, 3D Woven fabrics, in *Woven Fabrics*, edited by HY Jeon (InTech-Open Access Publisher), 2012.

6 Stig F, *3D-woven Reinforcement in Composites*, PhD thesis, KTH School of Engineering Sciences, Stockholm, Sweden, 2012.

7 Khokar N, *Making the Uniaxial Noobing Process Industrially Relevant*, paper presented at the 5th World Conference on 3D) Fabrics and Their Applications, New Delhi, 16 December 2013.

8 Bogdanovich A E, Karahan M, Lomov S V & Verpoest I, *Mech Mater*, 62(2013) 14.

9 Shigang A, Xiaolei Z, Yiqi M, Yongmao P & Daining F, *Appl Compos Mater*, 20(2013).

10 Karahan M, Lomov S V, Bogdanovich A E & Verpoest I, *Compos Sci Technol*, 71(2011) 1961.

11 Mishra R, Militky J, Behera B K & Banthia V, *J Text Inst*, 103(2012) 1151.

12 Shi W, Hu H, Sun B & Gu B, *J Text Inst*, 102(2011) 875.

13 Jia X, Sun B & Gu B, *Int J Damage Mech*, 21(2012) 237.

14 Carvelli V, Pazmino J, Lomov S V & Verpoest I, *Compos Sci Technol*, 73(2012) 9.

15 Endruweit A, Gommer F & Long A C, *Composites: Part A*, 49(2013) 109.

16 Ghosh T K & Zhou N, *Indian J Fibre Text Res*, 28 (2003) 471.

17 Mirtsch M & Yadav A, *STAMPING J* , May 9 (2006).

18 Sorrentino L, Simeoli G, Iannace S & Russo P, *Composites Part B*, 76(2015) 201.

19 Raftoyiannis I G, *Open J Compos Mater*, 2(2012) 31.

20 Azzam A & Li W, *Global Conference on Polymer and Composite Materials (PCM 2014)*. DOI: 10.1088/1757-899X/62/1/012016.

21 Brinson H F & Brinson L C, *Polymer Engineering Science and Viscoelasticity: An Introduction* (Springer New York Heidelberg Dordrecht London), 2015.